INORGANIC CHEMISTRY FRONTIERS

RESEARCH ARTICLE

View Article Online
View Journal | View Issue

Cite this: *Inorg. Chem. Front.*, 2023, **10**, 4845

$Hg_3O_2(NO_3)F$: a mercury nitrate oxyfluoride with an unprecedented $[(Hg_3O_2F)^+]_\infty$ cationic framework and excellent optical anisotropy†

Yi-Lei Lv,[a] Lei Huai,[a] Yu-Long Wei,[a] Liang Ma,[a] Yue-Qi Wei,[a] Wenlong Liu[a] and Ru-Ling Tang *[a,b]

Received 19th June 2023,
Accepted 10th July 2023

DOI: 10.1039/d3qi01146a

rsc.li/frontiers-inorganic

Combining multiple anions to design compounds with novel structures and excellent optical properties has become a hot research field. In this paper, a novel nitrate oxyfluoride, $Hg_3O_2(NO_3)F$, has been obtained. $Hg_3O_2(NO_3)F$ features an unprecedented $[(Hg_3O_2F)^+]_\infty$ cationic framework constructed by V-shaped HgO_2 units and original HgO_2F_2 tetrahedra and with isolated NO_3^- anions balancing the charge. $Hg_3O_2(NO_3)F$ is the first nitrate oxyfluoride containing a d^{10} metal. Importantly, $Hg_3O_2(NO_3)F$ exhibits superior optical anisotropy with the calculated birefringence of Δn = 0.23 at 1064 nm. Based on the theoretical calculation analyses, the good optical anisotropy is mainly derived from the well-arranged V-shaped HgO_2 units. This work proves that the strategy of introducing heteranions is effective for exploring high-performance optical materials.

Introduction

Developing inorganic compounds with novel crystal structures has aroused widespread concern. The combination of two or more kinds of anion groups to design compounds with interesting structure types is a favorable and fruitful route.[1–32] These new crystals may synergize the properties of multiple anions and can be potential candidates in some application fields including birefringence, nonlinear optics, fluorescence, and catalysis. Based on the structure performance relationship, many research systems focusing on optical performance have been developed in recent years.[33] It is well known that deep investigations have been performed on borate, phosphate, and chalcogenide compounds for nonlinear optics. However, in the last few years, some heteranions including halogen anions and O^{2-} anions, especially the F^- anion, have been widely introduced into oxate systems forming some promising research topics in nonlinear optics and birefringent materials, such as fluorooxoborates or borate fluorides, phosphate halides, and oxysulfides.[34] Some compounds derived from the above mixed anion systems exhibit excellent linear and nonlinear optical properties, such as AB_4O_6F (A = NH_4, Na, Rb, and Cs), $Pb_2(BO_3)(NO_3)$, $Sr_6Cd_2Sb_6O_7S_{10}$ and Sn_2PO_4I.[35–39]

Nitrate compounds, with a π-conjugated system, also have received intensive attention for their diverse optical properties. For instance, $RE(OH)_2NO_3$ (RE = La, Y, and Gd), $Rb_2Na(NO_3)_3$, $Sr_2(OH)_3NO_3$ and $Pb_{16}(OH)_{16}(NO_3)_{16}$ are good nonlinear optical crystals.[40–43] During the past few years, nitrates containing halogen atoms have aroused the enthusiasm of researchers due to their multifunctional optical performances. Until now, about forty-five inorganic nitrates containing halogen atoms have been reported (Table S3†). In the class of nitrates containing fluoride atoms, $Pb_2(NO_3)_2(H_2O)F_2$ shows the largest second harmonic generation (SHG) effect (12 × KH_2PO_4) and a very large birefringence (0.23 @1064 nm).[44] Besides, $Rb_3SbF_3(NO_3)_3$, $(NH_4)_3SbF_3(NO_3)_3$ and $Rb_2SbF_3(NO_3)_2$, also exhibit good SHG effects.[45–47] Moreover, nitrate halides including $Cs_2Pb(NO_3)_2Br_2$ and $CsHgNO_3Cl_2$ show good optical anisotropy.[48,49] It follows that the incorporation of halogen anions in nitrates enriches the structure diversity and can provide more promising optical materials. While, based on the survey of nitrates containing halogen atoms, intensive investigations have been performed on compounds comprising metal cations (Pb^{2+}, Sn^{2+}, Sb^{3+}) with lone pair electrons, which is beneficial for achieving favorable SHG effects and optical anisotropy,[28,39,45] other metal cations including d^0 and d^{10} metals which can also produce large polarizability have been less explored. Hence, further explorations are necessary for nitrate halides.

Besides the metal cations with lone pair electrons, Hg^{2+} has received widespread attention. It can form diverse coordi-

[a]*School of Chemistry and Chemical Engineering, Yangzhou University, Yangzhou, Jiangsu 225002, P. R. China. E-mail: rltang@yzu.edu.cn*
[b]*State Key Laboratory of Structural Chemistry, Fujian Institute of Research on the Structure of Matter, Chinese Academy of Sciences, Fuzhou, 350002, P. R. China*

†Electronic supplementary information (ESI) available: Additional tables and figures. CCDC 2268674. For ESI and crystallographic data in CIF or other electronic format see DOI: https://doi.org/10.1039/d3qi01146a

nation configurations including linear, trigonal-planar, or tetrahedral units, which are widely used to construct excellent NLO and birefringent materials, such as $HgBr_2$, β-HgBrCl, $LiHgPO_4$, Ag_2HgI_4, Ba_2HgTe_5 and trigonal HgS.[50–57] As mentioned, $CsHgNO_3Cl_2$ is a good birefringent crystal.[50] However, Hg-based nitrates with halogen anions are very rare: only $CsHgNO_3Cl_2$, $HgINO_3$ and $Ag_2HgI_2(NO_3)_2{\cdot}H_2O$ have been reported.[49,55,58] Therefore, we mainly focused on the research of Hg-based nitrate halides for developing compounds with novel structures and promising optical performances.

Here, a new Hg-based nitrate fluoride, $Hg_3O_2(NO_3)F$, has been obtained through a simple hydrothermal reaction method. In this work, we discuss the synthesis, crystal structure and comparison, optical performances, and the structure–property relationship based on theoretical calculations of $Hg_3O_2(NO_3)F$.

Experimental section

Synthesis

Caution! HF solution is highly corrosive! Proper protective equipment is essential for safety. LiF (Damas, 99.9%), $Hg(NO_3)_2{\cdot}H_2O$ (Damas, 99%), GeO_2 (Damas, 99%), and HF (Aladdin, 40% aqueous solution) without any further purification, were used to synthesize $Hg_3O_2(NO_3)F$ *via* a hydrothermal reaction. A mixture of 1 mmol of LiF (5.939 mg), 0.5 mmol of GeO_2 (52.32 mg) and 1 mmol of $Hg(NO_3)_2{\cdot}H_2O$ (281.62 mg) was weighed and poured into 20 mL Teflon liners, with 0.2 mL of HF and 3 mL of deionized water as a solvent for the reaction. The reaction temperature was set at 200 °C with a heating rate of 1 °C per minute from room temperature, which was maintained for three days, and then cooled to room temperature at the rate of 2 °C per hour. The yield of this compound is about 70% based on LiF.

Crystal structure determination

The single crystal X-ray diffraction (SXRD) of $Hg_3O_2(NO_3)F$ was performed using a Bruker D8 QUEST X-ray diffractometer, Mo Kα radiation (λ = 0.71073 Å). The direct method was used to record data, and then F^2 was performed with SHELX-2014 software and Olex2.[59] for the full-matrix least squares fitting process, and the correctness of the structure was checked using the PLATON program, and no problems were found.[60] The crystallographic data and refinement parameters of $Hg_3O_2(NO_3)F$ are shown in Table 1. Atomic coordinates, equivalent isotropic parameters, and selected bonds and angles are shown in Tables S1 and S2 (ESI†). The CIF document for $Hg_3O_2(NO_3)F$ is stored in the CCDC at number 2268674.†

Energy-dispersive X-ray spectroscopy (EDS)

EDS analysis was performed on several selected crystals using a Bruker quantum dispersive X-ray spectroscope. The data has proved the presence of elements Hg, N, O and F in the crystal, and the ratio is close to that from crystal structure determination (Fig. S4†).

Table 1 Crystal data and structure refinement parameters for $Hg_3O_2(NO_3)F$

Empirical formula	$Hg_3O_2(NO_3)F$
Formula weight	714.78
Temperature/K	296(2)
Crystal system	Orthorhombic
Space group	*Pnma*
a/Å	7.5474(10)
b/Å	10.99033(14)
c/Å	6.9906(9)
Volume/Å^3	579.86(13)
Z	4
ρ_{calc}/g cm^{-3}	8.188
μ/mm^{-1}	79.215
F(000)	1184.0
Crystal size/mm^3	0.15 × 0.13 × 0.1
Radiation	Mo Kα (λ = 0.71073)
2Θ range for data collection/°	6.908 to 59.308
Index ranges	$-10 \le h \le 10$, $-15 \le k \le 13$, $-9 \le l \le 9$
Reflections collected	5163
Independent reflections	857 [R_{int} = 0.0536, R_{sigma} = 0.0371]
Data/restraints/parameters	857/46/68
Goodness-of-fit on F^2	1.086
Final *R* indexes [$I \ge 2\sigma(I)$][a,b]	R_1 = 0.0237, wR_2 = 0.0494
Final *R* indexes [all data][a,b]	R_1 = 0.0290, wR_2 = 0.0510
Largest diff. peak/hole/e Å^{-3}	1.62/−1.61

[a] $R_1 = ||F_o| - |F_c||/|F_o|$. [b] $wR_2 = [w(F_o^2 - F_c^2)^2]/[w(F_o^2)^2]^{1/2}$.

Powder X-ray diffraction (PXRD)

A Bruker D8 Advance diffractometer with Cu-Kα radiation (λ = 1.5406 Å) was used for PXRD experiments on $Hg_3O_2(NO_3)F$ powder samples. The 2θ range is 10–70°, the step size is 0.02°, and the scanning rate of each step is 1s. The Mercury v3.8 program was used to obtain a simulated PXRD map of the single crystal structure data of $Hg_3O_2(NO_3)F$. The purity of the powder sample was confirmed by PXRD analysis (Fig. 1).

Infrared (IR) and UV-vis-NIR diffuse reflectance spectra

The infrared spectra of the powder samples were characterized in the range of 400–4000 cm^{-1} using a Magna 750 FI-IR spectrometer and using KBr pure powder samples as a reference. With $BaSO_4$ powder as the background, $Hg_3O_2(NO_3)F$ UV-vis-NIR

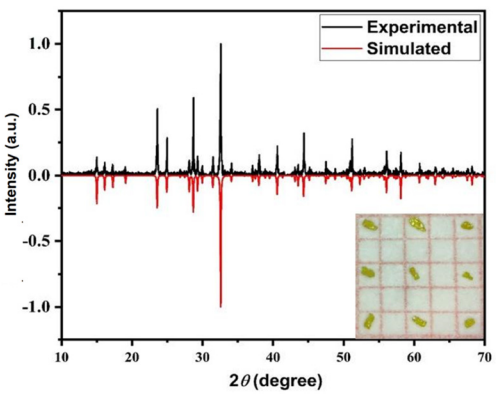

Fig. 1 Experimental and simulated powder XRD patterns of $Hg_3O_2(NO_3)F$.

diffuse reflection data in the range of 200–1200 nm was recorded on a Carry 5000 spectrometer. The Kubelka–Munk function was used to obtain diffuse reflection, and direct extrapolation methods were used to derive the band gap.

Thermogravimetric analysis

The thermal properties in flowing N_2 gas were determined on the Netzsch STA 449 F3 thermal analyzer. The powder samples were placed in an alumina crucible and heated from 20 to 1000 °C at a rate of 15 °C min^{-1}.

Theoretical calculation

The CASTP model based on the density functional theory (DFT) method was used to analyze the electronic structure and optical properties.[61–63] The Perdew–Burke–Ernzerhof (PBE) functional and generalized gradient approximation (GGA) were used for exchange correlation as valence electrons, considering the following orbital electrons: Hg: $5d^{10}6s^2$, N: $2s^22p^3$, O: $2s^22p^4$, F: $2s^22p^5$. The cut-off energies of $Hg_3O_2(NO_3)F$ were set to 850 eV, and the Monkhorst–Pack *k*-point grids were 3 × 2 × 4. The cut-off energies of $Hg_3O_2(NO_3)_2$ were set to 340 eV, and the Monkhorst–Pack *k*-point grids were 4 × 2 × 2.[64–66]

Results and discussion

Crystal structure

$Hg_3O_2(NO_3)F$ belongs to the orthorhombic system with the space group *Pnma* (No. 62). The asymmetrical unit contained two unique Hg, one unique F, one N, and four O atoms (Fig. 2a). In particular, the π-conjugated NO_3 unit is semi-occupied at the crystallographic site. The crystal structure of $Hg_3O_2(NO_3)F$ consists of planar π-conjugated NO_3^- anion units and a $[(Hg_3O_2F)^+]_\infty$ cationic framework. In the crystal structure of $Hg_3O_2(NO_3)F$, one N atom is coordinated with three O atoms forming an isolated NO_3 plane triangle (Fig. S3†) with N–O bond distances ranging from 1.24 to 1.26 Å and bond angles within the range of 119.6–120.2°. A Hg(1) atom is connected with two O(1) and two F(1) atoms to build a $Hg(1)O_2F_2$ tetrahedron (Fig. 2a). However, Hg(2) is surrounded by two O(1) atoms to form a V-shaped $Hg(2)O_2$ unit. The Hg(1)–O(1), Hg(2)–O(1) and Hg(1)–F(1) bond distances are 2.12, 2.067 and 2.38 Å. The O–Hg–O angles are 116.7 and 177.6°, the angles of F–Hg–O are 88.9 and 90.46°, and the F–Hg–F angles are 133.47° (Table S1†). $Hg(1)O_2F_2$ tetrahedra and V-shaped $Hg(2)O_2$ units are interconnected *via* a corner-shared O(1) atom to construct $(Hg_3O_2F_2)_\infty$ layers with a honeycomb feature in the bc plane (Fig. 2c). Furthermore, these $(Hg_3O_2F_2)_\infty$ layers are linked together *via* sharing of F atoms along the *a* axis to form the whole $[(Hg_3O_2F)^+]_\infty$ cationic framework, and the NO_3^- anions act as the counter ions to balance the charge (Fig. 2b). All the bond distances and bond angles are close to some reported compounds.[48,49,67]

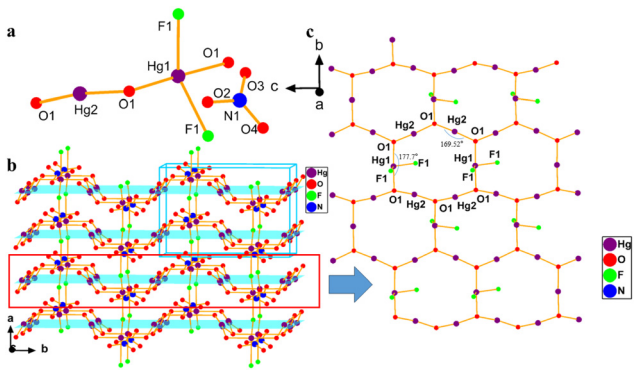

Fig. 2 (a) Coordination geometry of $Hg_3O_2(NO_3)F$; (b) the whole structure of $Hg_3O_2(NO_3)F$; (c) the $(Hg_3O_2F_2)_\infty$ layer.

To date, there are less than fifty inorganic nitrate halides, among which twenty-five nitrate fluorides have been studied (Table S3†). About the mercury-based nitrate halides, only $CsHgNO_3Cl_2$, $HgINO_3$ and $Ag_2HgI_2(NO_3)_2{\cdot}H_2O$ have been reported.[49,55,58] Hence $Hg_3O_2(NO_3)F$ is the first mercury-based nitrate containing F. In the crystal structure of $CsHgNO_3Cl_2$, the Hg atom adopts a high coordination configuration of a HgO_6Cl_2 polyhedron and further connects with NO_3 groups through the shared O atoms to form a $[HgNO_3Cl_2]^-$ anionic layer.[49] $HgINO_3$ features a neutral 2D framework with interconnected HgO_4I_2 and NO_3 units.[55] However, $Ag_2HgI_2(NO_3)_2{\cdot}H_2O$ shows a 3D network with Hg atoms connected to O atoms from NO_3 units and I atoms to form HgO_6I_2 polyhedra.[60] The coordination mode of Hg atoms is similar to that in $CsHgNO_3Cl_2$ and the NO_3 units are also disordered.[49] Moreover, $Hg_3O_2(NO_3)F$ can be regarded as the equivalent anion substitution from the compound $Hg_3O_2(NO_3)_2$.[69] With NO_3^- anion in $Hg_3O_2(NO_3)_2$ being replaced by one F^- anion, the symmetry has been changed from orthorhombic *Pbca* to *Pnma* of $Hg_3O_2(NO_3)F$. The coordination modes of the Hg atoms in $Hg_3O_2(NO_3)_2$ change from the original three kinds of V-shaped HgO_2 units to two kinds of different Hg-based units including tetrahedral $Hg(1)O_2F_2$ and V-shaped $Hg(2)O_2$ units. The unit cell parameters are a = 6.98; b = 13.56; c = 15.43; V = 1463.17; and Z = 8 for $Hg_3O_2(NO_3)_2$. It is evident that the unit cell parameters of b, c, Z, and V decreased compared with that of $Hg_3O_2(NO_3)F$, which may be induced by the smaller space occupancy of F^- than NO_3^- anions. In the crystal structure of $Hg_3O_2(NO_3)_2$ (Fig. S1†), the HgO_2 units are interconnected with each other to build two corrugated Hg_3O_2 honeycomb nets with isolated NO_3 units to balance the charge. The difference is that although both compounds exhibit a cellular framework and the NO_3 unit is separated, the cellular network is different and connected by a shared F atom in $Hg_3O_2(NO_3)F$. The introduction of the F atom causes the repeating unit to change from Hg_3O_2 to $Hg_3O_2F_2$, and the original two-dimensional structure to a three-dimensional structure, with F atoms participating in the connection of the $(Hg_3O_2F_2)_\infty$ layers. The distance between the layers decreases from 7.03 in $Hg_3O_2(NO_3)_2$ to 4.11 Å in $Hg_3O_2(NO_3)F$. The arrangement of NO_3^- has also transformed, from one half of them being located between the nets and the other half almost in the interstices of the nets, to all of it being near the nets. The hon-

eycomb pattern on the layer changes from being arranged along the ac plane to being arranged along the bc plane. The introduction of F atom reorganizes the structure and produces new chemical structures. The O–Hg–O angles of $Hg_3O_2(NO_3)_2$ are in the range from 167 (2) to 177.6 (2)° which are less than the O–Hg–O angles in $Hg_3O_2(NO_3)F$ and the honeycomb nets are not completely spread out on a plane (Fig. S1†).[69] All Hg-based nitrates are centric compounds, possibly because the arrangements of structural units are very symmetrical in three dimensions. Specifically, the orientations of NO_3 groups are antiparallel, leading to the cancellation of polarities, which is more likely to form compounds with centric crystal structures. The crystal structures of $HgINO_3$ and $CsHgNO_3Cl$ can prove this statement.[49,55] To sum up, $Hg_3O_2(NO_3)F$ exhibits a novel structure in nitrates and presents the first nitrate oxyfluoride containing d^{10} metal. Moreover, the tetrahedral HgO_2F_2 unit is reported for the first time in the title compound. In addition, it is very rare for a nitrate system to contain MO_xF_y fluoro-oxygen units, such as $Pb_2(NO_3)_2(H_2O)F_2$ and $PbCdF(SeO_3)(NO_3)$.[44,46]

Optical measurements

Based on the UV-vis-NIR spectrum (Fig. 3) of $Hg_3O_2(NO_3)F$ and the Kubelka–Munk function, the practical band gap of $Hg_3O_2(NO_3)F$ is 2.19 eV. The band gap of $Hg_3O_2(NO_3)F$ is relatively smaller compared with other nitrate halides including $Cs_2Pb(NO_3)_2Br_2$ (3.01 eV) and $CsHgNO_3Cl_2$ (3.1 eV).[48,49] There are no obvious vibration peaks at the range of 1500–4000 cm^{-1} in the IR spectra (Fig. 4). The intense band at 1315 cm^{-1} is attributable to the N–O stretching vibrations in the NO_3 triangles and the band at 804 cm^{-1} is ascribed to the nonplanar bending vibrations of the NO_3 planar groups. The peaks at 705 cm^{-1} and 673 cm^{-1} are attributed to the symmetric and asymmetric stretching of Hg–F bonds according to some previous literature. The peaks at 588 cm^{-1} and 522 cm^{-1} are attributed to the symmetric and asymmetric stretching of Hg–O bonds according to some previous literature.[48,49,68]

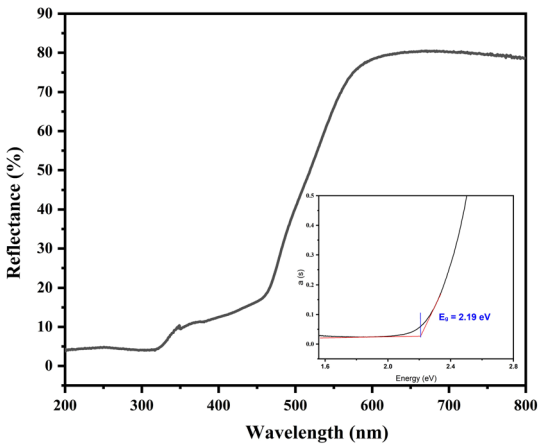

Fig. 3 UV-vis-NIR diffuse reflectance spectrum of $Hg_3O_2(NO_3)F$.

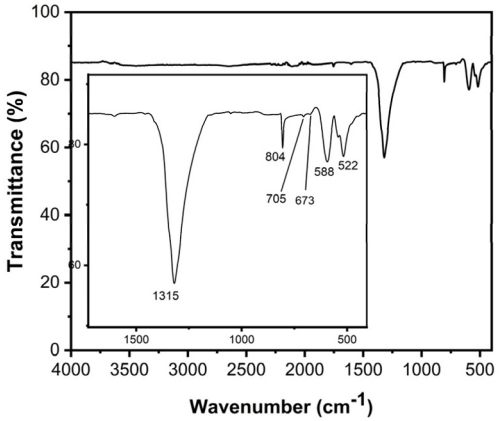

Fig. 4 IR spectrum of $Hg_3O_2(NO_3)F$.

Thermal stability

Fig. 5 shows the DTA curves of $Hg_3O_2(NO_3)F$. We can see that $Hg_3O_2(NO_3)F$ can be stable below 236 °C, and then in the range of 236–1000 °C, weight loss can be divided into several steps.[48,49]

Theoretical studies

In order to better elaborate the structure–performance relationship, first-principles calculations are carried out. The calculated band structure of $Hg_3O_2(NO_3)F$ indicates that the compound has a direct band gap of 1.12 eV (Fig. 6a). Due to the limitation of the exchange and correlation functions of GGA-PBE, the calculated band gap value is less than the experimental value, so a scissor operator of 1.07 eV is used to calculate the optical properties of $Hg_3O_2(NO_3)F$. For $Hg_3O_2(NO_3)F$, the top of valence bands (VBs) are mainly contributed by O-2p and parts of F-2p and Hg-5d (Fig. 6b). The bottom of conduction bands (CBs) are mainly occupied by the Hg-6s and O-2p orbitals. From the DOS diagram of this study, it can be seen that F contributes very little to the optical properties of the compound, which may be the reason for its small band gap. We can improve the band gap by introducing alkali metal,

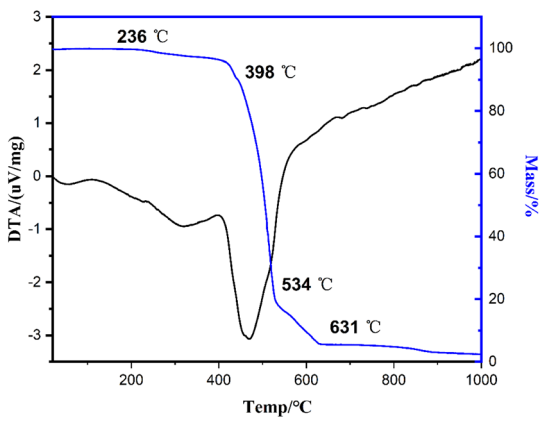

Fig. 5 TG–DSC curves of $Hg_3O_2(NO_3)F$.

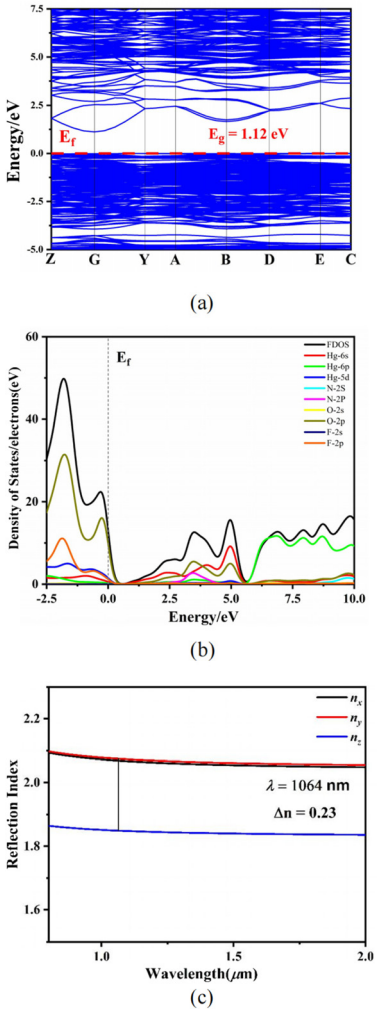

Fig. 6 (a) Calculated band gap; (b) density of states (DOS). The Fermi level is set at 0 eV; and (c) calculated refractive index dispersion curves of $Hg_3O_2(NO_3)F$.

alkaline earth or alkaline elements, or increasing the proportion of F atoms, as well as adjusting the proportions of F^- and NO_3^- anions. In summary, we conclude that the charge transfer between valence and conduction bands is mainly determined by Hg, O and F atoms. The calculated band gap of $Hg_3O_2(NO_3)_2$ is 1.16 eV (Fig. S2a†), which is close to the calculated value of $Hg_3O_2(NO_3)F$. According to the total and partial densities of states, the optical properties of $Hg_3O_2(NO_3)_2$ are mainly determined by Hg, and O atoms (Fig. S2b†).[69]

$Hg_3O_2(NO_3)F$ crystallizes in an orthogonal crystal system, which belongs to a biaxial crystal. The refractive index curves are calculated in Fig. 6c, showing a trend of $n_y > n_x > n_z$ in the wavelength range. The birefringence of $Hg_3O_2(NO_3)F$ at 1064 nm is calculated to be 0.23, which is the maximum among the nitrates which have been investigated on birefringence. The birefringence of $Hg_3O_2(NO_3)F$ is significantly enhanced compared with that of the mercury-based nitrate halide $CsHg(NO_3)Cl_2$ (0.145@1064 nm), and is larger than that

Table 2 Birefringence comparison of inorganic nitrates

Compounds	Birefringence	Ref.
$Hg_3O_2(NO_3)F$	0.23@1064 nm	This Work
$Pb_2(NO_3)_2(H_2O)F_2$	0.23@1064 nm	44
$(NH_4)_3SbF_4(NO_3)_2$	0.164@546 nm	47
$Cs_2Pb(NO_3)_2Br_2$	0.147@546 nm	48
$CsHgNO_3Cl_2$	0.145@546 nm	49
$Na_3Rb_6(CO_3)_3(NO_3)_2Cl{\cdot}(H_2O)_6$	0.14@546 nm	73
$Bi_3TeO_6OH(NO_3)_2$	0.115@1064 nm	10
$Gd(NO_3)(Se_2O_5){\cdot}3H_2O$	0.109@1064 nm	71
$(NH_4)_3SbF_3(NO_3)_3$	0.098@546 nm	47
$Ba_2NO_3(OH)_3$	0.082@532 nm	72
$Rb_2SbF_3(NO_3)_2$	0.06@1064 nm	46
$PbCdF(SeO_3)(NO_3)$	0.055@1064 nm	47
$RbSnF_2NO_3$	0.05@1064 nm	45
$Pb_{16}(OH)_{16}(NO_3)_{16}$	0.0365@700 nm	44

of other nitrate halides (Table 2), including $Cs_2Pb(NO_3)_2Br_2$ (0.147@546 nm), $(NH_4)_3SbF_4(NO_3)_2$ (0.164@546 nm), $(NH_4)_3SbF_3(NO_3)_3$ (0.098@546 nm), $PbCdF(SeO_3)(NO_3)$ (0.055@1064 nm), and $Hg_3O_2(NO_3)_2$ (0.123@1064 nm).[46–49,69] In addition, the birefringence of $Hg_3O_2(NO_3)F$ is equal to that of $Pb_2(NO_3)(H_2O)F$. $Pb_2(NO_3)(H_2O)F$ shows excellent optical anisotropy, which is induced by the synergistic effect of the NO_3 groups and lone pair electrons, combined with the superimposed enhanced polarization of PbO_9F_2 polyhedrons.[46,48,49] It is well-known that the anisotropic polarizability of the NO_3 anion is the largest in the planar triangular anion groups including BO_3, CO_3 and NO_3.[47,48,70,71] However, for $Hg_3O_2(NO_3)F$, the NO_3 units are not ideally arranged. Hence, the main contribution for optical anisotropy may be from the Hg-based units.

In order to further comprehend the contribution of each group to the favourable optical anisotropy of $Hg_3O_2(NO_3)F$, calculations of the electronic density difference map of $Hg_3O_2(NO_3)F$ have been performed. As exhibited in Fig. 7, even though the NO_3 units are not non-parallelly arranged, which has less contribution to the excellent linear optical properties, the electron cloud of Hg^{2+} shows nice interactions with O^{2-} and the polarizabilities of Hg–O bonds in the bc plane are stronger than that of the Hg–F bonds along the *a* axis, resulting the large optical anisotropy of $Hg_3O_2(NO_3)F$. Therefore, the

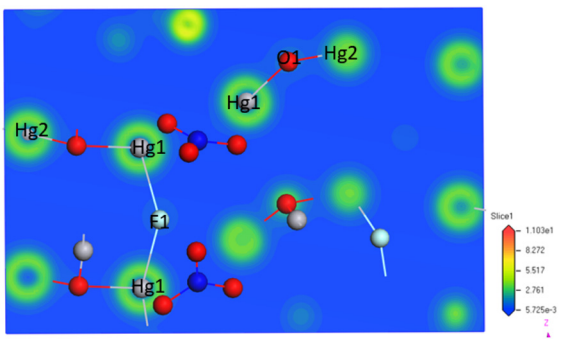

Fig. 7 Electron–density difference map of $Hg_3O_2(NO_3)F$. The Fermi level is set to 0 eV.

electron density difference map of $Hg_3O_2(NO_3)F$ further confirms that the excellent optical anisotropy mainly come from the Hg-based units (Fig. 7).[29] The enhanced birefringence of $Hg_3O_2(NO_3)F$ compared with that of $Hg_3O_2(NO_3)_2$ may come from the more ideal arrangements of HgO_2 units in plane and additional polarizability of the Hg–F bonds. It can be seen from Table S4† that many Hg-based compounds exhibit large birefringence, especially most of them built with Hg-based units with low coordination numbers. The large birefringence may be derived from the larger polarizabilities and suitable arrangements of these units.

Conclusions

The first mercury nitrate oxyfluoride, $Hg_3O_2(NO_3)F$, was discovered *via* a simple hydrothermal reaction. $Hg_3O_2(NO_3)F$ is the first nitrate oxyfluoride containing a d^{10} metal and shows a novel crystal structure. Besides, $Hg_3O_2(NO_3)F$ exhibits outstanding optical anisotropy among nitrates mainly induced by V-shaped HgO_2 units with high polarizabilities based on the analyses of theoretical calculations. The discovery of $Hg_3O_2(NO_3)F$ greatly enriches the family of nitrate compounds and may pave new avenues for the synthesis of mixed anion compounds. Further research will be carried out for investigating nitrate halides with diverse crystal structures and large birefringence.

Conflicts of interest

The authors declare that they have no conflict of interest.

Acknowledgements

The authors acknowledge the financial support from the National Natural Science Foundation of China (22101248), the National Key Laboratory Development Fund (20210002), and the Lvyangjinfeng Talent Program of Yangzhou (YZLYJFJH2021YXBS083). We thank Doctor Chun-Li Hu of the Fujian Institute of Research on the Structure of Matter, Chinese Academy of Sciences for the help with theoretical calculations.

References

1 C. C. Jin, X. P. Shi, H. Zeng, S. J. Han, Z. Chen, Z. H. Yang, M. Mutailipu and S. L. Pan, Hydroxyfluorooxoborate Na$[B_3O_3F_2(OH)_2][B(OH)_3]$: Optimizing the Optical Anisotropy with Heteroanionic Units for Deep Ultraviolet Birefringent Crystals, *Angew. Chem., Int. Ed.*, 2021, **60**, 20469–20475.

2 C. C. Jin, F. Li, B. L. Cheng, H. T. Qiu, Z. H. Yang, S. L. Pan and M. Mutailipu, Double-Modification Oriented Design of a Deep-UV Birefringent Crystal Functionalized by $[B_{12}O_{16}F_4(OH)_4]$ Clusters, *Angew. Chem., Int. Ed.*, 2022, **61**, e202203984.

3 J. Y. Guo, A. Tudi, S. J. Han, Z. H. Yang and S. L. Pan, $Sn_2B_5O_9Cl$: A Material with Large Birefringence Enhancement Activated Prepared via Alkaline-Earth-Metal Substitution by Tin, *Angew. Chem., Int. Ed.*, 2019, **58**, 17675–17678.

4 X. H. Dong, L. Huang, H. M. Zeng, Z. Lin, K. M. Ok and G. H. Zou, High-Performance Sulfate Optical Materials Exhibiting Giant Second Harmonic Generation and Large Birefringence, *Angew. Chem., Int. Ed.*, 2022, **61**, e202116790.

5 Y. L. Deng, L. Huang, X. H. Dong, L. Wang, K. M. Ok, H. M. Zeng, Z. Lin and G. H. Zou, $K_2Sb(P_2O_7)F$: Cairo Pentagonal Layer with Bifunctional Genes Reveal Optical Performance, *Angew. Chem., Int. Ed.*, 2020, **59**, 21151–21156.

6 Y. C. Yang, X. Liu, C. F. Zhu, L. Zhu, L. M. Wu and L. Chen, Inorganic Solid-State Nonlinear Optical Switch with a Linearly Tunable Tc Spanning a Wide Temperature Range, *Angew. Chem., Int. Ed.*, 2023, **62**, e202301404.

7 S. D. Yang, C. S. Lin, H. X. Fan, K. C. Chen, G. Zhang, N. Ye and M. Luo, Polar Phosphorus Chalcogenide Cage Molecules: Enhancement of Nonlinear Optical Properties in Adducts, *Angew. Chem., Int. Ed.*, 2023, **62**, e202218272.

8 J. H. Jiao, M. Zhang and S. L. Pan, Aluminoborates as Nonlinear Optical Materials, *Angew. Chem., Int. Ed.*, 2023, **62**, e202217037.

9 W. F. Zhou, B. X. Li, W. L. Liu and S. P. Guo, AAg_2PS_4 (A = K, Na/K): the first-type of noncentrosymmetric alkali metal Ag-based thiophosphates exhibiting excellent second-order nonlinear optical performances, *Inorg. Chem. Front.*, 2022, **9**, 4990–4998.

10 S. G. Zhao, Y. Yang, Y. G. Shen, B. Q. Zhao, L. Li, C. M. Ji, Z. Y. Wu, D. Q. Yuan, Z. S. Lin, M. C. Hong and J. H. Luo, Cooperation of Three Chromophores Generates the Water-Resistant Nitrate Nonlinear Optical Material $Bi_3TeO_6OH(NO_3)_2$, *Angew. Chem., Int. Ed.*, 2017, **56**, 540–544.

11 Z. Z. Zhang, Y. Wang, B. B. Zhang, Z. H. Yang and S. L. Pan, Polar Fluorooxoborate, NaB_4O_6F: A Promising Material for Ionic Conduction and Nonlinear Optics, *Angew. Chem., Int. Ed.*, 2018, **57**, 6577–6581.

12 R. Q. Wang, F. Liang, F. K. Wang, Y. W. Guo, X. Zhang, Y. Xiao, K. Bu, Z. S. Lin, J. Y. Yao, T. Y. Zhai and F. Q. Huang, $Sr_6Cd_2Sb_6O_7S_{10}$: Strong SHG Response Activated by Highly Polarizable Sb/O/S Groups, *Angew. Chem., Int. Ed.*, 2019, **58**, 8078–8081.

13 X. Huang, S. H. Yang, X. H. Li, W. L. Liu and S. P. Guo, $Eu_2P_2S_6$: The First Rare-Earth Chalcogenophosphate Exhibiting Large Second-Harmonic Generation Response and High Laser-Induced Damage Threshold, *Angew. Chem., Int. Ed.*, 2022, **61**, e202206791.

14 B. Achenbach, E. S. Svensson Grape, M. Wahiduzzaman, S. K. Pappler, M. Meinhart, R. Siegel, G. Maurin, J. Senker, A. K. Inge and N. Stock, Porous Salts Containing Cationic Al_{24}-Hydroxide-Acetate Clusters from Scalable, Green and

Aqueous Synthesis Routes, *Angew. Chem., Int. Ed.*, 2023, e202218679.

15 S. Bai, D. Wang, H. K. Liu and Y. Wang, Recent advances of oxyfluorides for nonlinear optical applications, *Inorg. Chem. Front.*, 2021, **8**, 1637–1654.

16 Y. Chi, J. Xu, H. G. Xue, Y. P. Zhang, X. L. Chen, M. H. Whangbo, S. P. Guo and S. Q. Deng, Triple-Kagome-Layer Slabs of Mixed-Valence Rare-Earth Ions Exhibiting Quantum Spin Liquid Behaviors: Synthesis and Characterization of $Eu_9MgS_2B_{20}O_{41}$, *J. Am. Chem. Soc.*, 2019, **141**, 9533–9536.

17 G. P. Han, B. H. Lei, Z. H. Yang, Y. Wang and S. L. Pan, A Fluorooxosilicophosphate with an Unprecedented SiO_2F_4 Species, *Angew. Chem., Int. Ed.*, 2018, **57**, 9828–9832.

18 Z. Q. Xie, M. Mutailipu, G. J. He, G. P. Han, Y. Wang, Z. H. Yang, M. Zhang and S. L. Pan, A Series of Rare-Earth Borates $K_7MRE_2B_{15}O_{30}$ (M = Zn, Cd, Pb; RE = Sc, Y, Gd, Lu) with Large Second Harmonic Generation Responses, *Chem. Mater.*, 2018, **30**, 2414–2423.

19 S. P. Guo, Y. Chi and H. G. Xue, $SnI_4{\cdot}(S_8)_2$: A Novel Adduct-Type Infrared Second-Order Nonlinear Optical Crystal, *Angew. Chem., Int. Ed.*, 2018, **57**, 11540–11543.

20 P. F. Li, C. L. Hu, F. Kong and J. G. Mao, The First UV Nonlinear Optical Selenite Material: Fluorination Control in $CaYF(SeO_3)_2$ and $Y_3F(SeO_3)_4$, *Angew. Chem., Int. Ed.*, 2023, **62**, e202301420.

21 J. H. Wu, B. Zhang, T. K. Jiang, F. Kong and J. G. Mao, From $Cs_8Sb_4Nb_5O_5F_{35}$ to $Cs_6Sb_4Mo_3O_5F_{26}$: The first non-centrosymmetric fluoroantimonite with d^0 transition metal, *Chin. J. Struct. Chem.*, 2023, **42**(1), 100016.

22 M. Yang, W. D. Yao, W. L. Liu and S. P. Guo, The first quaternary rare-earth oxythiogermanate with second-harmonic generation and ferromagnetic behavior, *Chem. Commun.*, 2023, **59**, 3894–3897.

23 M. Yang, Z. H. Shi, W. D. Yao and S. P. Guo, Second-Harmonic-Generation-Active Oxyhalides: $CuSb_2O_3X$ (X = Cl, Br), *Inorg. Chem.*, 2022, **61**, 42–46.

24 M. Yan, R. L. Tang, W. F. Zhou, W. L. Liu and S. P. Guo, Pb_3SBrI_3: the first Pb-based chalcohalide with multiple halogens features a unique two-dimensional structure composed of diverse Pb-centered polyhedra, *Dalton Trans.*, 2022, **51**, 12921–12927.

25 X. Lian, Z. T. Lu, W. D. Yao, S. H. Yang, W. L. Liu, R. L. Tang and S. P. Guo, Structural Transformation and Second-Harmonic-Generation Activity in Rare-Earth and d^0 Transition-Metal Oxysulfides $RE_3NbS_3O_4$ (RE = Ce, Sm, Gd, Dy), *Inorg. Chem.*, 2021, **60**, 10885–10889.

26 X. Huang, S. H. Yang, W. Liu and S. P. Guo, $Ba_3HgGa_2S_7$: A Zero-Dimensional Quaternary Sulfide Featuring a Unique $[Hg_2Ga_4S_{14}]^{12-}$ String and Exhibiting a High Photocurrent Response, *Inorg. Chem.*, 2022, **61**, 12954–12958.

27 R. L. Tang, Y. L. Wei, Y. Chi, Z. H. Shi, W. L. Liu and S. P. Guo, Cation Regulation to Investigate the Chalcogenide Borate $RE_6Nb_2MgSB_8O_{26}$ (RE = La-Nd) Family, *Inorg. Chem.*, 2022, **61**, 8653–8661.

28 M. Yan, R. L. Tang, W. L. Liu and S. P. Guo, From $Ba_3Nb_2O_2F_{12}(H_2O)_2$ to $Ba_{0.5}NbO_2F_2(H_2O)$: Achieving Balanced Nonlinear Optical Performance by O/F Ratio Regulation, *Inorg. Chem.*, 2022, **61**, 20709–20715.

29 R. L. Tang, G. X. Liu, W. D. Yao, L. N. Zhang, W. L. Liu and S. P. Guo, $BaSc_2(HPO_3)_4(H_2O)_2$: a new nonlinear optical phosphite exhibiting a 3D $\{[Sc_2(HPO_3)_4]^{2-}\}_\infty$ anionic framework and phase-matchable SHG effect, *Inorg. Chem. Front*, 2022, **9**, 5377–5385.

30 M. Yang, W. L. Liu and S. P. Guo, Sb_5O_7I: Exploration of Ternary Antimony-Based Oxyhalide as a Nonlinear-Optical Material, *Inorg. Chem.*, 2022, **61**, 14517–14522.

31 M. Yan, Z. D. Sun, W. D. Yao, W. F. Zhou, W. L. Liu and S. P. Guo, A highly distorted HgS_4 tetrahedron-induced moderate second-harmonic generation response of $EuHgGeS_4$, *Inorg. Chem. Front.*, 2020, **7**, 2451–2458.

32 Y. Chi, H. G. Xue and S. P. Guo, Designing Sulfide Borate as a Novel Type of Second-Order Nonlinear-Optical Material, *Inorg. Chem.*, 2020, **59**, 1547–1555.

33 M. Gai, Y. Wang, T. Tong, Z. Yang and S. L. Pan, $ZnIO_3F$: Zinc Iodate Fluoride with Large Birefringence and Wide Band Gap, *Inorg. Chem.*, 2020, **59**, 4172–4175.

34 R. L. Tang, M. Yan, W. D. Yao, W. L. Liu and S. P. Guo, $HgTeO_2F(OH)$: A Nonlinear Optical Oxyfluoride Constructed of Active $[TeO_2F(OH)]^{2-}$ Pyramids and V-Shaped $[HgO_2]^{2-}$ Groups, *Inorg. Chem.*, 2022, **61**, 2333–2339.

35 Y. Pan, S. P. Guo, B. W. Liu, H. G. Xue and G. C. Guo, Second-order nonlinear optical crystals with mixed anions, *Coord. Chem. Rev.*, 2018, **374**, 464–496.

36 X. F. Wang, Y. Wang, B. B. Zhang, F. F. Zhang, Z. H. Yang and S. L. Pan, CsB_4O_6F: A Congruent-Melting Deep-Ultraviolet Nonlinear Optical Material by Combining Superior Functional Units, *Angew. Chem., Int. Ed.*, 2017, **56**, 14119–14123.

37 G. Q. Shi, Y. Wang, F. F. Zhang, B. B. Zhang, Z. H. Yang, X. L. Hou, S. L. Pan and K. R. Poeppelmeier, Finding the Next Deep-Ultraviolet Nonlinear Optical Material: $NH_4B_4O_6F$, *J. Am. Chem. Soc.*, 2017, **139**, 10645–10648.

38 J. L. Song, C. L. Hu, X. Xu, F. Kong and J. G. Mao, A Facile Synthetic Route to a New SHG Material with Two Types of Parallel π-Conjugated Planar Triangular Units, *Angew. Chem.*, 2015, **127**, 3750–3753.

39 J. Y. Guo, A. Tudi, S. J. Han, Z. H. Yang and S. L. Pan, Sn_2PO_4I: An Excellent Birefringent Material with Giant Optical Anisotropy in Non π-Conjugated Phosphate, *Angew. Chem., Int. Ed.*, 2021, **60**, 24901–24904.

40 Y. X. Song, M. Luo, C. S. Lin and N. Ye, Structural Modulation of Nitrate Group with Cations to Affect SHG Responses in $RE(OH)_2NO_3$ (RE = La, Y, and Gd): New Polar Materials with Large NLO Effect after Adjusting pH Values of Reaction Systems, *Chem. Mater.*, 2017, **29**, 896–903.

41 G. H. Zou, C. S. Lin, H. Kim, H. Jo and K. Ok, $Rb_2Na(NO_3)_3$: A Congruently Melting UV-NLO Crystal with a Very Strong Second-Harmonic Generation Response, *Crystals*, 2016, **6**, 42.

42 S. Dill, K. Gibson, J. Glaser, S. Tragl and H. J. Meyer, Synthese and Struktur der basischen Erdalkalinitrate $Sr_2(OH)_3NO_3$ and $Ba_2(OH)_3NO_3$, *Z. Anorg. Allg. Chem.*, 2007, **633**, 274–279.

43 L. X. Chang, L. Wang, X. Su, S. L. Pan, R. Hailili, H. W. Yu and Z. H. Yang, A nitrate nonlinear optical crystal $Pb_{16}(OH)_{16}(NO_3)_{16}$ with a large second-harmonic generation response, *Inorg. Chem.*, 2014, **53**, 3320–3325.

44 G. Peng, Y. Yang, Y. H. Tang, M. Luo, T. Yan, Y. Q. Zhou, C. S. Lin, Z. S. Lin and N. Ye, Collaborative enhancement from Pb^{2+} and F^- in $Pb_2(NO_3)_2(H_2O)F_2$ generates the largest second harmonic generation effect among nitrates, *Chem. Commun.*, 2017, **53**, 9398–9401.

45 L. Wang, H. M. Wang, D. Zhang, D. J. Gao, J. Bi, L. Huang and G. H. Zou, Centrosymmetric $RbSnF_2NO_3$. noncentrosymmetric $Rb_2SbF_3(NO_3)_2$, *Inorg. Chem. Front.*, 2021, **8**, 3317–3324.

46 Y. X. Ma, C. L. Hu, B. X. Li, F. Kong and J. G. Mao, PbCdF$(SeO_3)(NO_3)$: A Nonlinear Optical Material Produced by Synergistic Effect of Four Functional Units, *Inorg. Chem.*, 2018, **57**, 11839–11846.

47 Q. Wang, J. Ren, D. Wang, L. Cao, X. Dong, L. Huang, D. Gao and G. H. Zou, Low temperature molten salt synthesis of noncentrosymmetric $(NH_4)_3SbF_3(NO_3)_3$ and centrosymmetric $(NH_4)_3SbF_4(NO_3)_2$, *Inorg. Chem. Front.*, 2023, **10**, 2107–2114.

48 Y. Long, X. H. Dong, H. M. Zeng, Z. Lin and G. H. Zou, Layered Perovskite-like Nitrate $Cs_2Pb(NO_3)_2Br_2$ as a Multifunctional Optical Material, *Inorg. Chem.*, 2022, **61**, 4184–4192.

49 Y. Long, X. H. Dong, L. Huang, H. M. Zeng, Z. Lin and G. H. Zou, $CsHgNO_3Cl_2$: A New Nitrate UV Birefringent Material Exhibiting an Optimized Layered Structure, *Inorg. Chem.*, 2020, **59**, 12578–12585.

50 Y. Y. Dang, X. G. Meng, K. Jiang, C. Zhong, X. G. Chen and J. G. Qin, A promising nonlinear optical material in the Mid-IR region: new results on synthesis, crystal structure and properties of noncentrosymmetric β-HgBrCl, *Dalton Trans.*, 2013, **42**, 9893–9897.

51 B. L. Wu, C. L. Hu, F. F. Mao, R. L. Tang and J. G. Mao, Highly Polarizable Hg^{2+} Induced a Strong Second Harmonic Generation Signal and Large Birefringence in $LiHgPO_4$, *J. Am. Chem. Soc.*, 2019, **141**, 10188–10192.

52 C. Yang, X. Liu, C. L. Teng, Q. Wu and F. Liang, Acentric Organic-Inorganic Hybrid Halide $[N(CH_3)_4]_2HgBr_2I_2$ Featuring an Isolated $[HgBr_2I_2]^{2-}$ Tetrahedron and Second-Order Nonlinearity, *Inorg. Chem.*, 2021, **60**, 6829–6835.

53 Q. Wu, C. Yang, J. Ma, X. Liu and Y. J. Li, Halogen-Ion-Induced Structural Phase Transition Giving a Polymorph of $HgBr_2$ with Balanced Nonlinear Optical Properties, *Inorg. Chem.*, 2021, **60**, 19297–19303.

54 C. Yang, X. Liu, C. Teng, X. Cheng, F. Liang and Q. Wu, Hierarchical molecular design of high-performance infrared nonlinear Ag_2HgI_4 material by defect engineering strategy, *Mater. Today Phys.*, 2021, **19**, 100432.

55 K. Persson and B. Holmberg, Structure of Mercury(II) Iodide Nitrate, *Acta Crystallogr.*, 1982, **38**, 900–903.

56 M. Sun and J. Yao, Ba_2HgTe_5: a Hg-based telluride with giant birefringence induced by linear $[HgTe_2]$ units, *Inorg. Chem. Front.*, 2022, **9**, 5024–5031.

57 M. Yan, W. D. Yao, W. L. Liu, R. L. Tang and S. P. Guo, Helical $\{[HgS]\}_n$ Chain-Induced Balanced Nonlinear-Optical Performance for Trigonal Mercury Sulfide, *Inorg. Chem.*, 2021, **60**, 16917–16921.

58 K. Penneth and B. Holmbeerg, Structure of Mercury Disilver Diiodide Dinitrate Monohydrate, *Acta Crystallogr.*, 1982, **38**, 904–907.

59 V. Dolomanov, L. J. Bourhis, R. J. Gildea, J. A. K. Howard and H. Puschmann, OLEX2: A complete structure solution, refinement and analysis program, *J. Appl. Crystallogr.*, 2009, **42**, 339–341.

60 J. Tauc, R. Grigorovici and A. Vancu, Optical Properties and Electronic Structure of Amorphous Germanium, *Phys. Status Solidi B*, 1966, **15**, 627–637.

61 S. K. Kurtz and T. T. Perry, A Powder Technique for the Evaluation of Nonlinear Optical Materials, *J. Appl. Phys.*, 1968, **39**, 3798–3813.

62 S. J. Clark, M. D. Segall, C. J. Pickard, P. J. Hasnip, M. J. Probert, K. Refson and M. C. Z. Payne, First Principles Methods Using CASTEP, *Z. Kristallogr. – Cryst. Mater.*, 2005, **220**, 567–570.

63 D. D. Macdonald and M. Urquidi-Macdonald, Application of Kramers-Kronig Transforms in the Analysis of Electrochemical Systems: I. Polarization Resistance, *J. Electrochem. Soc.*, 1985, **132**, 2316–2319.

64 X. Lian, W. D. Yao, W. L. Liu, R. L. Tang and S. P. Guo, KNa_2ZrF_7: A Mixed-Metal Fluoride Exhibits Phase-Matchable Second-Harmonic-Generation Effect and High Laser-Induced Damage Threshold, *Inorg. Chem.*, 2021, **60**, 19–23.

65 J. P. Perdew and M. Levy, Physical Content of the Exact Kohn-Sham Orbital Energies: Band Gaps and Derivative Discontinuities, *Phys. Rev. Lett.*, 1983, **51**, 1884–1887.

66 R. L. Tang, W. Xu, W. J. Xie and C. L. Hu, $Sc_2F_2(B_2O_5)$: a deep ultraviolet scandium borate fluoride exhibiting large birefringence induced by the synergistic effect of B_2O_5 and ScO_nF_2 groups, *Inorg. Chem. Front.*, 2022, **9**, 5153–5160.

67 H. Marc and S. Dieter, Phase diagrams and structures of HgX_2 (X = I, Br, Cl, F), *C. R. Chim.*, 2005, **8**, 147–156.

68 J. F. Rooms, A. V. Wilson, I. Harvey, A. J. Bridgeman and N. A. Young, Mercury-fluorine interactions: a matrix isolation investigation of $Hg\cdots F_2$, HgF_2 and HgF_4 in argon matrices, *Phys. Chem. Chem. Phys.*, 2008, **10**, 4594–4605.

69 H. Behm, Trimereury Dinitrate Dioxide, $Hg_3O_2(NO_3)_2$, *Acta Crystallogr., Sect. C: Cryst. Struct. Commun.*, 1983, **39**, 1319–1321.

70 D. Yan, M. M. Ren, Q. Liu, F. F. Mao, Y. Ma, R. L. Tang, H. B. Huang, B. B. Zhang, X. D. Zhang and S. F. Li, $[C(NH_2)_2NHNO_2][C(NH_2)_3](NO_3)_2$: A Mixed Organic Cationic Hybrid Nitrate with an Unprecedented Nonlinear-Optical-Active Unit, *Inorg. Chem.*, 2023, **62**, 4757–4761.

71 C. Wu, L. H. Li, L. Lin, Z. P. Huang, M. G. Humphrey and C. Zhang, $Gd(NO_3)(Se_2O_5)\cdot 3H_2O$: a nitrate-selenite nonlinear optical material with a short ultraviolet cutoff edge, *Dalton Trans.*, 2020, **49**, 3253–3259.
72 X. H. Dong, L. Huang, Q. Y. Liu, H. M. Zeng, Z. Lin, D. G. Xu and G. H. Zou, Perfect balance harmony in $Ba_2NO_3(OH)_3$: a beryllium-free nitrate as a UV nonlinear optical material, *Chem. Commun.*, 2018, **54**, 5792–5795.
73 M. Cheng, W. Q. Jin, Z. H. Yang and S. L. Pan, Large optical anisotropy-oriented construction of a carbonate-nitrate chloride compound as a potential ultraviolet birefringent material, *Chem. Sci.*, 2022, **13**, 13482–13488.